Molecular Crystals and Liquid Crystals
Publication details, including instructions for authors and subscription information:
http://www.tandfonline.com/loi/gmcl20

Thermal and Optical Properties of Self-Assembly Systems: Two Pairs of Distinct Structural Isomers

N. Pongali Sathya Prabu [a], V. N. Vijayakumar [a] & M. L. N. Madhu Mohan [a]

[a] Liquid Crystal Research Laboratory (LCRL), Bannari Amman Institute of Technology, Sathyamangalam, India

Available online: 20 Mar 2012

To cite this article: N. Pongali Sathya Prabu, V. N. Vijayakumar & M. L. N. Madhu Mohan (2012): Thermal and Optical Properties of Self-Assembly Systems: Two Pairs of Distinct Structural Isomers, Molecular Crystals and Liquid Crystals, 557:1, 144-160

To link to this article: http://dx.doi.org/10.1080/15421406.2012.640568

Mol. Cryst. Liq. Cryst., Vol. 557: pp. 144–160, 2012

ISSN: 1542-1406 print/1563-5287 online
DOI: 10.1080/15421406.2012.640568

Thermal and Optical Properties of Self-Assembly Systems: Two Pairs of Distinct Structural Isomers

N. PONGALI SATHYA PRABU, V. N. VIJAYAKUMAR, AND M. L. N. MADHU MOHAN*

Liquid Crystal Research Laboratory (LCRL), Bannari Amman Institute of Technology, Sathyamangalam, India

*Two homologous pairs of linear and bent structural isomers are isolated and characterized. The series, which is linear in shape, is comprised of double hydrogen bonds forming between hydroquinone and alkyloxy benzoic acid (HQ+n*OBA*) and hydroquinone and alky benzoic acids (HQ+n*BA*) respectively. The other series with the bent structure formed double hydrogen bonds between resorcinol and alkyloxy benzoic acid (Rl+n*OBA*) and resorcinol and alky benzoic acids (Rl+n*BA*) respectively. Thus two linear mesogen series HQ+n*OBA* and HQ+n*BA* and two bent homologous series Rl+n*OBA* and Rl+n*BA* are formed, which are referred as structural isomers. Formation of hydrogen bond is conformed by FTIR, while the proposed structure is conformed by proton and carbon NMR studies. Transition temperatures and phases have been identified by differential scanning calorimetry and optical polarizing microscopic studies. Phase diagrams have been constructed for all the homologous series. The homologous series with oxygen atom in benzoic acid moiety is observed to exhibit rich phase variance compared to the series without oxygen atom. Comparison of transition temperatures, occurrence of phases, and other related properties are discussed.*

Keywords Hydrogen bonded liquid crystals; isomers; NMR; phase diagrams

1. Introduction

Synthesis and characterization of self-assembly systems in liquid crystals referred as hydrogen bonding liquid crystals gained importance and paved way for new type of soft materials. Kato and his research group [1–17] investigated many such systems with complementary components. The self-assembly systems formed by alkyloxy carboxylic acids exhibit rich phase polymorphism. It has been earlier reported by us that these self-organized systems induce variety of new phenomena like reentrant phase occurrence [18,19], light modulation [20], optical shuttering action [21–24], and field-induced transitions [20,25,26].

The carboxylic acids with other acids are reported [18–26] to form complementary single and multiple hydrogen bonds. We have already reported [19,25] the ambient Smectic ordering observed in the hydrogen bonded complex formed between carboxylic acids and anilines, which individually exhibits mesogenic properties and in turn, the H-bonds have pronounced effect in bringing down the phase transition temperature. However, there

*Address correspondence to M. L. N. Madhu Mohan, Liquid Crystal Research Laboratory (LCRL), Bannari Amman Institute of Technology, Sathyamangalam 638 401, India. Tel.: +91 9442437480; Fax: +91 4295 223 775. E-mail: mln.madhu@gmail.com

are reports in the literature [27,28] to obtain mesogenic hydrogen bonded liquid crystals (HBLC); it is enough if one of the compounds exhibits mesogenic properties. It is a great surprise to note that a mesogenic HBLC can be formed through two non-mesogenic compounds [29,30] by hydrogen bonding. Thus, it can inferred that depending upon the position of the hydrogen bonding and chemical structure of the individual compounds, hydrogen bonding can induce liquid crystallinity and also plays a pivotal role in bringing down considerably the magnitude of the phase transition temperatures.

In the present work, a successful attempt has been made to design and isolate four homologous series of HBLC with linear and bent structures. The series, which is linear in shape, is comprised of double hydrogen bonds forming between hydroquinone and alkyloxy benzoic acid (HQ+*n*OBA) and hydroquinone and alky benzoic acids (HQ+*n*BA), respectively. The other series with the bent structure formed double hydrogen bonds between resorcinol and alkyloxy benzoic acid (Rl+*n*OBA) and resorcinol and alky benzoic acids (Rl+*n*BA), respectively. Thermal and optical properties exhibited by these mesogens are discussed and compared.

2. Experimental

Optical textural observations were made with a Nikon polarizing microscope equipped with Nikon digital CCD camera system with 5 mega pixels and 2560*1920 pixel resolutions. The liquid crystalline textures were processed, analyzed, and stored with the aid of ACT-2U imaging software system. The temperature control of the liquid crystal cell was equipped by Instec HCS402-STC 200 temperature controller (Instec, USA) to a temperature resolution of $\pm 0.1^{\circ}$C. This unit is interfaced to computer by IEEE–STC 200 to control and monitor the temperature. The liquid crystal sample is filled by capillary action in its isotropic state into a commercially available (Instec, USA) polyamide buffed cell with 5-micron spacer. The transition temperatures and corresponding enthalpy values were obtained by DSC (Shimadzu DSC-60, Japan). FTIR spectra was recorded (ABB FTIR MB3000) and analyzed with the MB3000 software. The ^{1}H NMR and ^{13}C NMR spectra were recorded by Bruker International Ultra shield instrument at 300 MHz. The *p*-*n*-alkyloxy benzoic acids (*n*OBA), *p*-*n*-alkyl benzoic acids (*n*BA), resorcinol (Rl), and hydroquinone (HQ) were supplied by Sigma Aldrich (Germany), and all the solvents used were HPLC grade.

3. Synthesis of HBLC

Linear intermolecular hydrogen bonded mesogens are synthesized by the addition of two moles of *n*OBA/*n*BA with one mole of HQ in *N*,*N*-Dimethyl formamide (DMF), respectively. Bent intermolecular hydrogen bonded mesogens are synthesized by the addition of two moles of *n*OBA/*n*BA with one mole of Rl in DMF, respectively.

Further, they are subject to constant stirring for 14 h at ambient temperature of 30°C till a white precipitate in a dense solution is formed. The white crystalline crude complexes so obtained by removing excess DMF are then recrystallized with dimethyl sulfoxide (DMSO) and the yield varied from 85% to 95%. Yield of higher homologues complexes are observed to be more compared to its lower counterparts. The molecular structure of the present linear homologous series of *n*OBA with HQ (HQ+*n*OBA) and *n*BA with HQ (HQ+*n*BA) are depicted in the Figures 1(a) and 1(b) respectively while the bent homologous series of *n*OBA with Rl (Rl+*n*OBA) and *n*BA with Rl (Rl+*n*BA) are depicted in the Figures 1(c) and 1(d) respectively, where *n* represents the alkyl and alkyloxy carbon number. In the

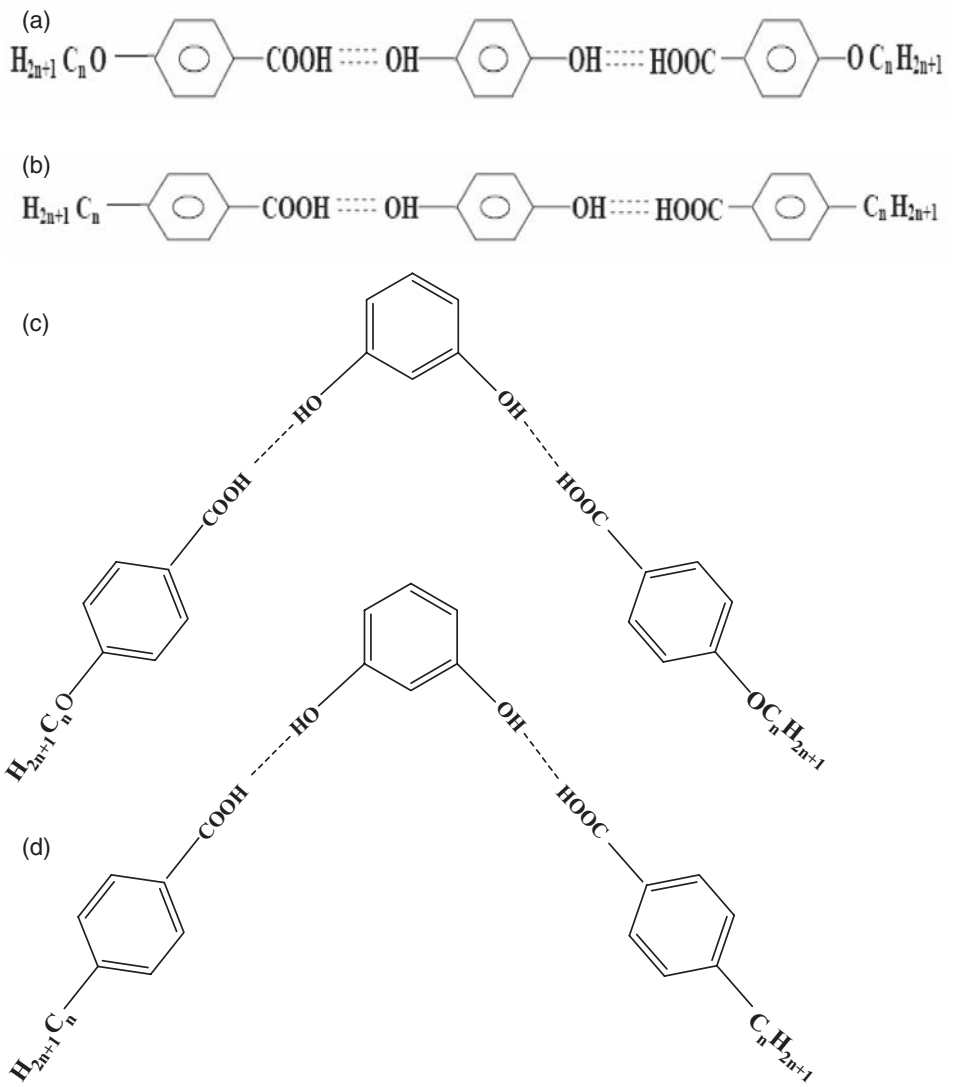

Figure 1. (**a**) Molecular structure of HQ+*n*OBA. (**b**) Molecular structure of HQ+*n*BA. (**c**) Molecular structure of Rl+*n*OBA. (**d**) Molecular structure of Rl+*n*BA.

above series, the alternate hydrogen bonded sites situated on either sides of benzene ring moiety of the HQ and Rl can be identified.

4. Results and Discussion

All the hydrogen bonded complexes isolated under the present investigation mostly are white crystalline solids and are stable at room temperature. They are insoluble in water and sparingly soluble in common organic solvents such as methanol, ethanol, and benzene and dichloro methane. However, they show a high degree of solubility in coordinating solvents

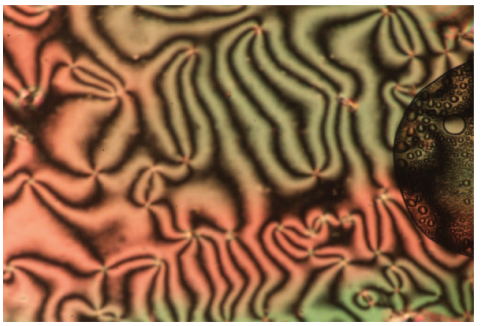

Plate 1. Threaded texture of Nematic.

like DMSO, DMF, and pyridine. They show high thermal and chemical stability when subjected to repeated thermal scans performed during POM and DSC studies.

5. Phase Identification

The observed phase variants, transition temperatures, and corresponding enthalpy values obtained by DSC in cooling and heating cycles for the HQ+*n*OBA, HQ+*n*BA, Rl+*n*OBA, and Rl+*n*BA series are presented in Tables 1–4 respectively.

*5.1. HQ+*n*OBA Homologous Series*

The mesogens of the *HQ*+n*OBA* homologous series are found to exhibit characteristic textures [31], viz., Nematic (threaded texture, Plate 1), Smectic C (broken focal conic texture, Plate 2), Smectic F (checkered board texture, Plate 3), and Smectic G (multicolored smooth mosaic texture, Plate 4), respectively. The general phase sequence of the *HQ*+n*OBA* in the cooling run can be shown as:

Isotropic → Nematic → Sm F → Crystal HQ+*n*OBA, where $n = 5$ and 6
Isotropic → Nematic → Sm C → Sm F → Crystal HQ+*n*OBA, where $n = 7$–9
Isotropic → Nematic → Sm C → Sm G → Crystal HQ+*n*OBA, where $n = 10$–12

Plate 2. Broken focal conic texture of Smectic C.

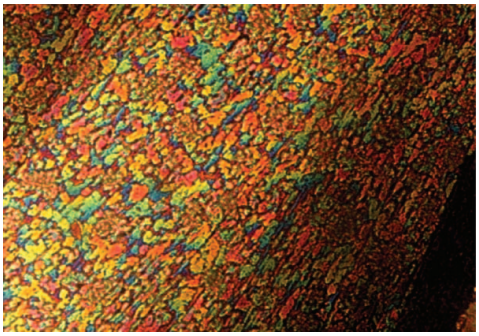

Plate 3. Checkered board texture of Smectic F.

*5.2. HQ+n**BA** Homologous Series*

The mesogens of the *HQ*+n*BA* homologous series are found to exhibit characteristic textures [31], viz., Nematic (threaded texture), Smectic F (chequered board texture), and Smectic G (multicolored smooth mosaic texture), respectively. The general phase sequence of the *HQ*+n*BA* in the cooling run can be shown as:

Isotropic → Sm G → Crystal HQ+*n*BA, where $n = 2$ and 3
Isotropic → Nematic → Sm F → Crystal HQ+*n*BA, where $n = 4$–8

*5.3. Rl+n**OBA** Homologous Series*

The mesogens of the Rl+n*OBA* homologous series are found to exhibit characteristic textures [31], viz., Nematic (threaded texture), Smectic C (broken focal conic texture), and Smectic F (checkered board texture), respectively. The general phase sequence of the Rl+n*OBA* in the cooling run can be shown as:

Isotropic → Sm F → Crystal Rl+5OBA
Isotropic → Nematic → Sm F → Crystal Rl+6OBA
Isotropic → Nematic → Sm C → Sm F → Crystal Rl+*n*OBA, where $n = 7$–12

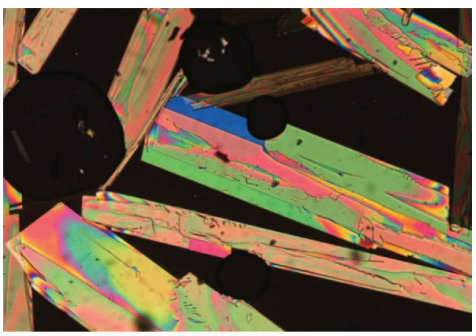

Plate 4. Multicolored smooth mosaic texture of Smectic G.

Table 1. Phase transition temperatures of HQ+*n*OBA obtained by various techniques along with enthalpy values in J/g

Complex	Phase variance	Study	Crystal to melt	N	C	F	Crystal
HQ+5BAO	NF	DSC (h)	125.3 (61.43)	131.9 (5.87)		#	
		DSC (c)		131.4 (2.09)		126.8 (13.9)	117.9 (66.23)
		POM (c)		131.8		127.4	118.4
HQ+6BAO	NF	DSC (h)	107.5 (34.26)	140.9 (0.29)		#	
		DSC (c)		136.8 (2.94)		123.3 (10.41)	93.1 (32.87)
		POM (c)		137.4		123.8	93.6
HQ+7BAO	NCF	DSC (h)	93.7 (72.76)	#	#	#	
		DSC (c)		124.3 (1.38)	105.4 (0.42)	87.6 (31.11)	73.7 (37.92)
		POM (c)		124.9	105.8	88.2	74.3
HQ+8BAO	NCF	DSC (h)	102.6 (24.33)	#	107.2 (1.34)	#	
		DSC (c)		130.3 (10.99)	103.3 (2.97)	96.1 (28.48)	52.9 (36.13)
		POM (c)		130.9	103.8	96.7	53.3
HQ+9BAO	NCF	DSC (h)	95.0 (76.03)	#	115.7 (3.67)	#	
		DSC (c)		121.1 (6.26)	111.2 (3.44)	89.8 (23.0)	66.6 (50.40)
		POM (c)		121.8	111.6	90.4	67.4
HQ+10BAO	NCF	DSC (h)	87.1 (65.01)	132.8 (12.36)	119.1 (3.76)	97.2 (34.41)	
		DSC (c)		128.4 (13.48)	115.3 (4.11)	91.5 (32.80)	73.8 (24.05)
		POM (c)		128.9	119.7	92.9	74.2
HQ+11BAO	NCF	DSC (h)	97.3 (93.56)	132.3 (8.65)	125.8 (4.66)	#	
		DSC (c)		128.2 (7.04)	121.7 (4.47)	84.9 (24.02)	78.0 (61.76)
		POM (c)		128.8	122.4	85.3	78.7
HQ+12BAO	NCF	DSC (h)	96.3 (97.89)	130.1 (19.31)	#	#	
		DSC (c)		130.1 (7.84)	124.8 (8.01)	119.9 (17.87)	86.7 (27.76)
		POM (c)		130.8	125.4	120.4	87.5

Note. # = Monotropic transition; (c) = Cooling run; (h) = Heating run.

Table 2. Phase transition temperatures of HQ+*n*BA obtained by various techniques with enthalpy values in J/g

Complex	Phase variance	Study	Crystal to melt	N	F	G	Crystal
HQ+2BA	G	DSC (h)	111.5 (55.67)			#	
		DSC (c)				118.4 (7.57)	105.6 (53.88)
		POM (c)				118.9	106.2
HQ+3BA	G	DSC (h)	136.5 (86.23)			#	
		DSC (c)				135.0 (13.21)	130.7 (80.82)
		POM (c)				135.6	131.1
HQ+4BA	NF	DSC (h)	101.1 (37.8)	#	#		
		DSC (c)		112.9 (3.92)	100.6 (3.39)		95.2 (42.69)
		POM (c)		113.5	100.9		95.7
HQ+5BA	NF	DSC (h)	89.2 (29.48)	#	#		
		DSC (c)		109.5 (0.33)	90.1 (1.57)		82.4 (28.76)
		POM (c)		110.1	90.8		82.9
HQ+6BA	NF	DSC (h)	94.1 (50.96)	#	#		
		DSC (c)		113.0 (9.41)	89.6 (merged with crystal)		87.9 (47.39)
		POM (c)		113.7	90.5		88.4
HQ+7BA	NF	DSC (h)	101.5 (45.08)	#	113.3 (1.43)		
		DSC (c)		122.8 (8.54)	108.8 (0.99)		96.0 (41.36)
		POM (c)		123.5	109.3		96.8
HQ+8BA	NF	DSC (h)	95.7 (62.86)		#		
		DSC (c)		102.6 (4.07)	93.1 (merged with crystal)		90.9 (48.24)
		POM (c)		103.1	101.9		91.4

Note. # = Monotropic transition; (c) = Cooling run; (h) = Heating run.

Table 3. Phase transition temperatures of Rl+*n*OBA obtained by various techniques with enthalpy values in J/g

Complex	Phase variance	Study	Crystal to melt	N	C	F	Crystal
Rl+5BAO	F	DSC (h)	119.5 (83.23)			#	
		DSC (c)				120.7 (7.11)	113.7 (86.61)
		POM (c)				121.3	114.2
Rl+6BAO	NF	DSC (h)	105.7 (36.15)	140.3 (0.27)		116.3 (0.08)	
		DSC (c)		138.7 (16.64)		114.3 (2.14)	93.9 (40.62)
		POM (c)		139.1		114.8	94.5
Rl+7BAO	NCF	DSC (h)	94.5 (101.96)	#	#	#	
		DSC (c)		104.2 (6.21)	90.6 (2.09)	87.2 (4.91)	64.8 (47.88)
		POM (c)		104.6	91.3	87.8	65.2
Rl+8BAO	NCF	DSC (h)	101.5 (35.44)	#	115.4 (2.11)	#	
		DSC (c)		134.2 (2.83)	112.1 (11.38)	99.5 (2.80)	95.4 (30.29)
		POM (c)		134.6	112.9	96.0	95.9
Rl+9BAO	NCF	DSC (h)	94.1 (73.34)	#	110.5 (2.41)	#	
		DSC (c)		128.9 (2.11)	107.4 (3.32)	90.3 (23.32)	67.6 (52.04)
		POM (c)		129.3	107.9	90.8	68.2
Rl+10BAO	NCF	DSC (h)	86.9 (38.86)	#	117.2 (6.24)	97.2 (20.33)	
		DSC (c)		133.1 (1.69)	112.5 (12.77)	91.4 (14.74)	74.5 (21.25)
		POM (c)		133.7	112.8	91.9	75.2
Rl+11BAO	NCF	DSC (h)	97.8 (120.92)	#	121.9 (1.01)	113.5 (4.92)	
		DSC (c)		134.3 (2.80)	118.7 (0.2)	112.6 (12.76)	85.6 (34.47)
		POM (c)		134.9	119.1	112.9	86.2
Rl+12BAO	NCF	DSC (h)	95.8 (81.26)	#	119.8 (16.9)	#	
		DSC (c)		123.8 (2.88)	115.7 (15.84)	109.4 (merged with crystal)	87.4 (25.2)
		POM (c)		124.3	116.2	109.9	88.1

#Monotropic transition, (c) Cooling run, (h) Heating run.

Table 4. Phase transition temperatures of Rl+*n*BA obtained by various techniques with enthalpy values in J/g

Complex	Phase variance	Study	Crystal to melt	G	Crystal
Rl+2BA	G	DSC (h)	103.8 (26.93)	#	
		DSC (c)		108.9 (1.15)	96.2 (24.43)
		POM (c)		109.4	96.8
Rl+3BA	G	DSC (h)	128.9 (41.25)	143.0 (0.72)	
		DSC (c)		138.0 (1.92)	123.4 (45.03)
		POM (c)		138.5	123.7
Rl+4BA	G	DSC (h)	94.2 (36.76)	#	
		DSC (c)		103.0 (6.26)	87.2 (40.04)
		POM (c)		103.6	87.9
Rl+5BA	G	DSC (h)	87.3 (25.67)	#	
		DSC (c)		85.9 (16.18)	82.3 (27.71)
		POM (c)		86.4	82.6
Rl+6BA	G	DSC (h)	92.8 (39.50)	#	
		DSC (c)		92.4 (3.87)	86.9 (48.22)
		POM (c)		92.8	87.3
Rl+7BA	G	DSC (h)	99.6 (59.68)	#	
		DSC (c)		104.1 (2.13)	94.9 (61.47)
		POM (c)		105.0	95.7
Rl+8BA	G	DSC (h)	98.3 (58.37)	#	
		DSC (c)		104.5 (1.34)	93.1 (58.91)
		POM (c)		104.9	93.8

Note. # = Monotropic transition; (c) = Cooling run; (h) Heating run.

*5.4. Rl+*n*BA Homologous Series*

The mesogens of the Rl+n*BA* homologous series are found to exhibit characteristic texture [31], viz., Smectic G (multicolored smooth mosaic texture). The general phase sequence of the Rl+n*BA* in the cooling run can be shown as:

Isotropic → Sm G→ Crystal Rl+*n*BA, where $n = 2$–8.

6. Spectroscopic Studies

6.1. Infrared Spectroscopy (FTIR)

IR spectra of free n*OBA*, HQ, Rl, and their respective intermolecular hydrogen bonded complexes are recorded in the solid state (KBr) at room temperature. Figure 2(a) illustrates the FTIR spectra of hydrogen bonded complex HQ+5OBA and HQ+5BA in solid state at room temperature as a representative case. Further, the presence of an intense peak at 1250 cm^{-1} in the HQ+5OBA and the absence of the same peak in corresponding hydrogen bonded HQ+5BA complex confirms [32] the skeletal vibrations of the above hydrogen bonded aromatic system.

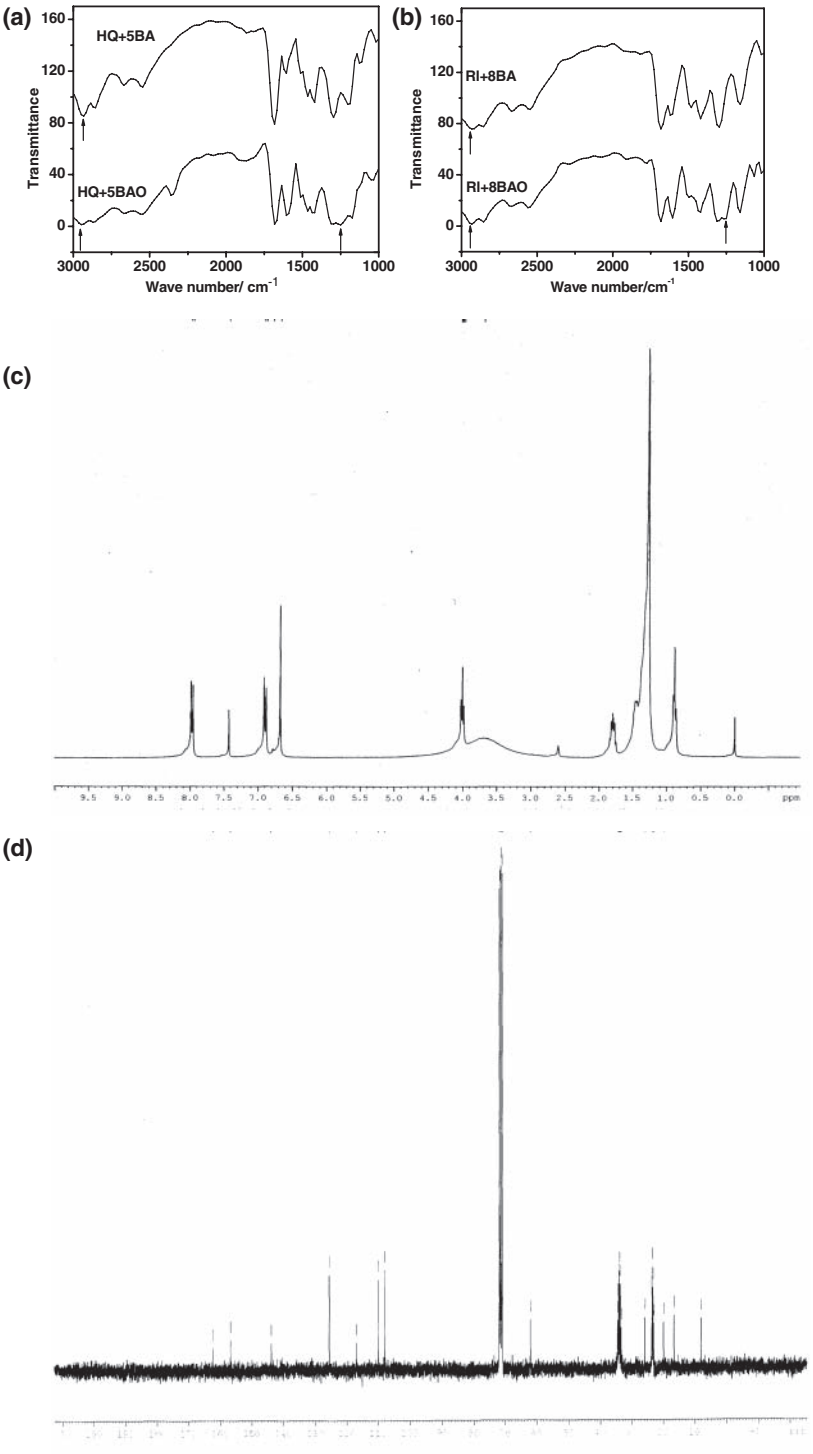

Figure 2. (**a**) FTIR spectra of HQ+5OBA and HQ+5BA. (**b**) FTIR spectra of Rl+8OBA and Rl+8BA. (**c**) ^{1}H NMR spectra of HQ+12OBA. (**d**) ^{13}C NMR spectra of HQ+12OBA.

Figure 2(b) illustrates the FTIR spectra of hydrogen bonded complex Rl+8OBA and Rl+8BA in solid state at room temperature as a representative case. Furthermore, the presence of an intense peak at 1248 cm^{-1} in the Rl+8OBA and the absence of the same peak in corresponding hydrogen bonded Rl+8BA complex confirms [32] the skeletal vibrations of the above hydrogen bonded aromatic system.

A noteworthy feature in the spectra of HQ+5OBA, HQ+5BA, Rl+8OBA, and Rl+8BA complexes is the appearance of the sharp high intense band at 2932 cm^{-1}, which clearly suggests the formation of hydrogen bond upon complexation.

6.2. ^{1}H NMR Studies

The proposed molecular structure is verified by the ^{1}H NMR studies. The^{1}H NMR spectra are recorded for all the synthesized complexes under present investigation. As a representative case, the spectrum of HQ+12BAO (Figure 2(c)) is discussed. ^{1}H NMR spectrum of the complex is recorded in $CDCl_3$ with tetramethylsilane (TMS) as the internal standard. The recorded spectrum is shown in Figure 2(c) and the following chemical shifts were observed.

(1) Broad resonance signals are observed approximately in the range of 0.5 ppm–2.8 ppm for the methylene group. In the HQ+12BAO complex, these signals are observed between 2.597 ppm and 0.856 ppm, which has been attributed to the existence of the backbone methylene.
(2) Sets of multiplets between 6.912 ppm–6.677 ppm, 7.428 ppm, and 7.991 ppm–7.962 ppm are assigned to aromatic protons.
(3) The existence of the methoxy proton unit resonance showed a signal between 3.668 ppm and 4.027 ppm.

The shifts obtained through ^{1}H NMR study are found in accordance to the proposed molecular structure.

6.3. ^{13}C NMR Studies

The projected organic molecular structure of the complex is verified through ^{13}C NMR study. The ^{13}C NMR spectra are recorded for all the synthesized complexes under present investigation. As a representative case, the spectrum of HQ+12BAO (Figure 2(d)) is discussed. This study infers the information regarding the number of non-equivalent carbons and also to identify the types of carbon atoms (methyl, methylene, aromatic, carbonyl, and so on). Hence the carbon skeleton of the organic molecule can be deduced completely with the aid of the ^{13}C NMR study.

^{13} C NMR spectrum of the complex was recorded in $CDCl_3$ with TMS as the internal standard. AS a representative case, the spectrum of HQ+12BAO is elaborately discussed. The recorded spectrum is shown as Figure 2(d) and the following chemical shifts are observed.

(1) Broad resonance magnetic signals are observed approximately in the range of 34.427 ppm–16.499 ppm, which contribute to the methylene carbon.
(2) A single signal shift achieved at 7.985 ppm is assigned to the methyl carbon.
(3) The existence of the alkyloxy carbon in the proposed molecule is confirmed by the shift observed at 71.716 ppm–62.040 ppm.

(4) Multiple resonance magnetic signals obtained at 125.607 ppm–107.839 ppm are due to the benzene carbon.
(5) The sharp signal obtained at 162.208 ppm is attributed to the carboxylic acid carbon.

Thus the proposed structure of the organic molecule is further confirmed with ^{13}C NMR studies.

7. DSC Studies

DSC thermograms are obtained in heating and cooling cycle. The sample is heated with a scan rate of 10°C min^{-1} and held at its isotropic temperature for 2 min so as to attain thermal stability. The cooling run is performed with a scan rate of 10°C min^{-1}. The respective equilibrium transition temperatures and corresponding enthalpy values of HQ+*n*OBA, HQ+*n*BA, Rl+*n*OBA, and Rl+*n*BA homologous series are listed separately in Tables 1–4 respectively. Polarizing optical microscopic studies also confirm these DSC transition temperatures.

8. Phase Diagram of Pure nOBA and nBA

The phase diagram of pure *n*OBA is reported [20,23] to be composed of two phases namely, Nematic and Smectic C while the phase diagram of pure *n*BA is reported [33] to be composed of only Nematic phase.

*8.1. Phase Diagram of HQ+*n*OBA*

Phase diagram of *HQ*+n*OBA* is depicted in Figure 3. The following points can be elucidated from this Figure 3.

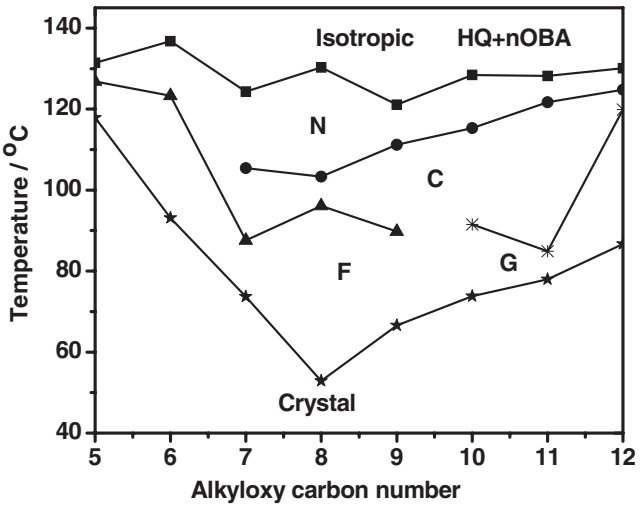

Figure 3. Phase diagram of HQ+*n*OBA.

(1) The HQ+*n*OBA hydrogen bonded homologous series exhibits orthogonal and titled phases namely Nematic and Smectic C, Smectic F, and Smectic G phases respectively.
(2) Total thermal range of the mesogenic phases increased with increase in the alkyloxy carbon number up to octyloxy carbon and then starts to decrease till dodecyloxy benzoic acid.
(3) Nematic phase is observed in all the complexes of the present homologous series.
(4) The Smectic C phase is induced in the higher homologous members from heptyloxy benzoic acid and continued till dodecyloxy carbon. The thermal phase width is largest for undecyloxy carbon and narrowest for dodecyloxy carbon.
(5) A higher ordered phase, Smectic G phase, is observed in HQ+10OBA complex quenching Smectic F phase thermal range.
(6) A systematic decrease in the crystallization temperatures is observed up to octyloxy benzoic carbon number upon which the crystallization temperatures start to increase proportionally along with its corresponding carbon number.
(7) One of the interesting observation in the present series is the detection of odd–even effect at isotropic to Nematic phase transition with respect to enthalpy values and the corresponding transition temperatures.

*8.2. Phase Diagram of HQ+*n*BA*

Phase diagram of HQ+*n*BA is depicted in Figure 4. The following points can be elucidated from this Figure 4.

(1) The HQ+*n*BA hydrogen bonded homologous series exhibits orthogonal and titled phases namely Nematic and Smectic F, and Smectic G phases respectively.
(2) Nematic phase is observed from carbon number 4 to 8 of the present homologous series.
(3) The Smectic F phase is induced from carbon number 4 to 8. The thermal phase width is largest for undecyloxy carbon and narrowest for dodecyloxy carbon.
(4) A higher ordered phase, Smectic G phase, is observed only in HQ+2BA complex.

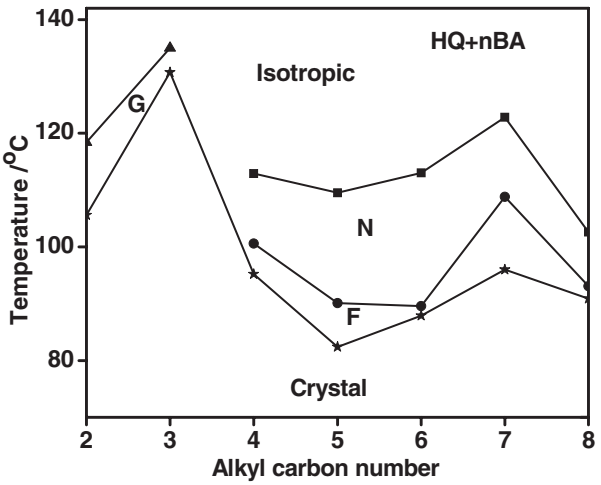

Figure 4. Phase diagram of HQ+*n*BA.

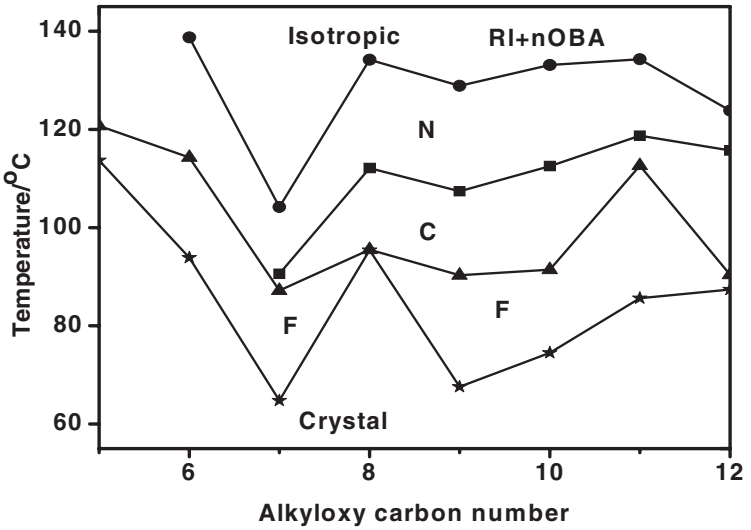

Figure 5. Phase diagram of Rl+*n*OBA.

8.3. Phase Diagram of Rl+nOBA

Phase diagram of Rl+n*OBA* is depicted in Figure 5. The following points can be elucidated from this Figure 5.

(1) The Rl+*n*OBA hydrogen bonded homologous series exhibits orthogonal and titled phases namely Nematic, Smectic C, and Smectic F phases respectively.
(2) Nematic phase is observed in almost all the complexes of the present homologous series except in the complex of carbon number 5.
(3) The Smectic C phase is induced from heptyloxy benzoic acid and continued till dodecyloxy carbon.
(4) One of the interesting observations in the present series is the detection of odd–even effect with respect to transition temperatures at isotropic to Nematic phase transition.

8.4. Phase Diagram of Rl+nBA

Phase diagram of Rl+*n*BA is depicted in Figure 6. The following points can be elucidated from this Figure 6.

(1) The Rl+*n*BA hydrogen bonded homologous series exhibits only Smectic G phases.
(2) Smectic G phase is observed in all the complexes of the present homologous series.
(3) The thermal phase span of Smectic G is almost unaltered throughout the series.

9. Positional Influence of Oxygen Atom

The positional influence of oxygen atom in HQ+*n*OBA and HQ+*n*BA, and Rl+*n*OBA and Rl+*n*BA is discussed with respect to phase occurrence and phase transition temperatures.

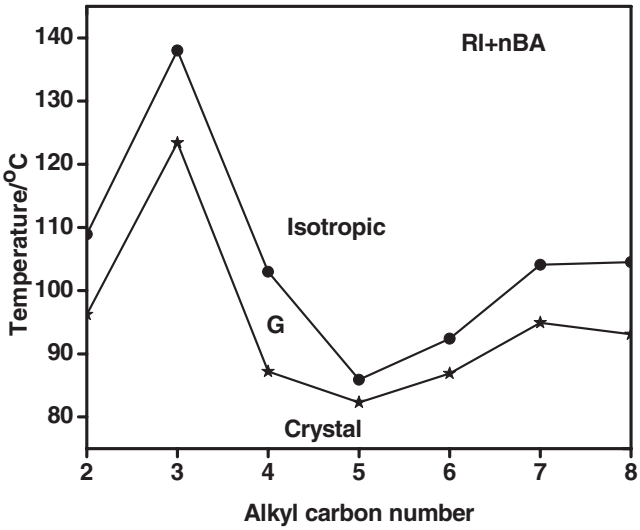

Figure 6. Phase diagram of Rl+*n*BA.

*9.1. Comparison of HQ+n**OBA** and HQ+n**BA** Homologues*

(1) In HQ+*n*OBA homologous series, the presence of oxygen atom enabled to induce Smectic C, which is a tilted phase, while in other members of the HQ+*n*BA series Smectic C is not observed.
(2) The odd–even effect is clearly seen in HQ+*n*OBA series at isotropic to Nematic temperatures while no such effect is observed in HQ+*n*BA.
(3) It is worth mentioning that in HQ+*n*OBA the lower alkyloxy carbon members exhibit Smectic F phase while Smectic F is quenched by Smectic G in the higher members. In contrary to this, in HQ+*n*BA the lower alkyl carbon members exhibit Smectic G phase while Smectic G is quenched by Smectic F in the higher members.
(4) The isotropic temperatures of various homologues in HQ+*n*OBA are higher compared to their counterparts in HQ+*n*BA. Thus, in general, the positional influence of the oxygen atom has reduced the isotropic temperatures considerably.
(5) The crystallization temperatures of various homologues in HQ+*n*OBA are around 80°C, which are comparatively much lower than that of homologues of HQ+*n*BA. Oxygen atom has increased the crystallization temperatures implying that the mesogen thermal range has been reduced.

*9.2. Comparison of Rl+n**OBA** and Rl+n**BA** Homologues*

(1) In the bent molecular structure, oxygen has considerably enhanced the mesogenic variance. Rl+*n*OBA exhibits tri-phase variance with Nematic and Smectic C and F phases while Rl+*n*BA exhibits mono-phase variant with Smectic G.
(2) The isotropic temperatures in Rl+*n*OBA are consistently high at around 140°C in most of the homologues while the isotropic temperatures are mostly at 100°C for Rl+*n*BA. Thus oxygen atom has influenced to increase the isotropic temperatures.
(3) Crystallization temperatures are below 80°C in Rl+*n*OBA series while they are above 80°C in Rl+*n*BA.

9.3. Discussion on Structural Isomerism

HQ+*n*OBA and Rl+*n*OBA, and HQ+*n*BA and Rl+*n*BA are two pairs of structural isomers with and without oxygen atom. HQ+*n*OBA and HQ+*n*BA (Figures 1(a), 1(b)) possess linear molecular structure while Rl+*n*OBA and Rl+*n*BA (Figures 1(c), 1(d)) exhibit bent molecular structure.

9.4. Comparison of Linear and Bent Molecular Structure

The mesogens with linear molecular structures exhibit usually traditional phases like Nematic and Smectic C, F, and G phases respectively. The respective phase diagrams along with transition temperatures are discussed in the above sections.

The mesogens with bent molecular structures exhibit phases like Nematic and Smectic C, F, and G phases respectively. It is worth mentioning that the bent mesogens are not exhibiting the expected bent textures. Furthermore, it is interesting to note that the occurrence of the phases in bent and linear mesogens are identical.

In the bent mesogens (Rl+*n*OBA, Rl+*n*BA), the influence of oxygen is predominant in the sense that without oxygen atom only higher ordered Smectic G phase is observed. However, in the linear mesogens (HQ+*n*OBA, HQ+*n*BA) the influence of oxygen is not so pronounced. Only Smectic C phase has been quenched in oxygen rich molecular structure compared to its counterpart with oxygen atom.

Acknowledgments

The authors acknowledge the financial support rendered by All India Council for Technical Education (AICTE), Department of Science and Technology (DST), and Defense Research Development Organization (DRDO), New Delhi. Infrastructural support provided by Bannari Amman Institute of Technology is gratefully acknowledged.

References

[1] Kihara, H., Kato, T., Uryu, T., & Frechet, J. M. J. (1996). *Chem. Mater.*, *8*, 961.
[2] Kato, T., & Frechet, J. M. J. (1995). *Macromol. Symp.*, *98*, 311.
[3] Kato, T., & Frechet, J. M. J. (1989). *J. Am. Chem. Soc.*, *111*, 8533.
[4] Kato, T., & Frechet, J. M. J. (1989). *Macromolecules*, *22*, 3818.
[5] Kato, T., Nakano, M., Moteki, T., Uryu, T., & Ujiie, S. (1995). *Macromolecules*, *28*, 8875.
[6] Kato, T., Frechet, J. M. J., Wilson, P. G., Saito, T., Uryu, T., Fujishima, A., Jin, C., & Kaneuchi, F. (1993). *Chem. Mater.*, *5*, 1094.
[7] Kato, T., Wilson, P. G., Fujishima, A., & Frechet, J. M. J. (1990). *Chem. Lett.*, 2003.
[8] Kato, T., Fukumasa, M., & Frechet, J. M. J. (1995). *Chem. Mater.*, *7*, 368.
[9] Fukumasa, M., Kato, T., Uryu, T., & Frechet, J. M. J. (1993). *Chem. Lett.*, 65.
[10] Kato, T., Fujishima, A., & Frechet, J. M. J. (1990). *Chem. Lett.*, 919.
[11] Kato, T., Adachi, H., Fujishima, A., & Frechet, J. M. J. (1992). *Chem. Lett.*, 265.
[12] Kato, T., Uryu, T., Kaneuchi, F., Jin, C., & Frechet, J. M. J. (1993). *Liq. Cryst.*, *14*, 1311.
[13] Kato, T., Kihara, H., Uryu, T., Ujiie, S., Limura, K., Frechet, J. M. J., & Kumar, U. (1993). *Ferroelectrics*, *148*, 161.
[14] Kumar, U., Frechet, J. M. J., Kato, T., Ujiie, S., & Limura, K. (1992). *Angew. Chem. Int. Ed. Engl.*, *31*, 1531.
[15] Kumar, U., Kato, T., & Frechet, J. M. J. (1992). *J. Am. Chem. Soc.*, *114*, 6630.
[16] Kato, T., Kihara, H., Uryu, T., Fujishima, A., & Frechet, J. M. J. (1992). *Macromolecules*, *25*, 6836.

[17] Kato, T., Kihara, H., Kumar, U., Uryu, T., & Frechet, J. M. J. (1994). *Angew. Chem. Int. Ed. Engl.*, *33*, 1644.
[18] Vijayakumar, V. N., Murugadass, K., & Madhu Mohan, M. L. N. (2010). *Mol. Cryst. Liq. Cryst.*, *517*, 41.
[19] Chitravel, T., & Madhu Mohan, M. L. N. (2010). *Mol. Cryst. Liq. Cryst.*, *524*, 131.
[20] Vijayakumar, V. N., & Madhu Mohan, M. L. N. (2010). *Mol. Cryst. Liq. Cryst.*, *517*, 113.
[21] Vijayakumar, V. N., & Madhu Mohan, M. L. N. (2009). *J. Opto. Elec. Adv. Mat.*, *11*, 1139.
[22] Vijayakumar, V. N., & Madhu Mohan, M. L. N. (2010). *Physica B*, *405*, 4418.
[23] Vijayakumar, V. N., & Madhu Mohan, M. L. N. (2009). *Sol. State Sci.*, *4*, 482.
[24] Vijayakumar, V. N., & Madhu Mohan, M. L. N. (2009). *Braz. J. Phys.*, *39*, 677.
[25] Vijayakumar, V. N., Murugadass, K., & Madhu Mohan, M. L. N. (2011). *Mol. Cryst. Liq. Cryst.*, *537*, 22.
[26] Vijayakumar, V. N., & Madhu Mohan, M. L. N. (2009). *Sol. State Comm.*, *149*, 2090.
[27] Tian, Y. Q., He, X., Zhao, Y. Y., Tang, X. Y., Jin Li, T., & Huang, X. M. (1998). *Mol. Cryst. Liq. Cryst.*, *309*, 19.
[28] Swathi, P., Kumar, P. A., Pisipati, V. G. K. M., Rajeshwari, A. V., Sreehari Sastry, S., & Murthy, P. N. (2002). *Z. Natur. Forsch*, *57a*, 797.
[29] Hentrich, F., Diele, S., & Tschierske, C. (1994). *Liq. Cryst.*, *17*, 827.
[30] Kobayashi, Y., & Matsunage, Y. (1987). *Bull. Chem. Soc. Jpn.*, *60*, 3515.
[31] Gray, G. W., & Goodby, J. W. G. (1984). *Smectic Liquid Crystals: Textures and Structures*, Leonard Hill: London.
[32] Nakamoto, K. (1978). *Infrared and Raman Spectra of Inorganic and Co-ordination Compounds*, Interscience: New York.
[33] Vijayalakshmi, K., & Sreehari Sastry, S. (2009). *Acta Phys. Pol. A*, *115*, 690.